ChemPubSoc Europe

DOI: 10.1002/celc.201402054

# Effects of Redox Mediators on the Catalytic Activity of Iron Porphyrins towards Oxygen Reduction in Acidic Media

Qinggang He,*[a] Gang Wu,[b] Ke Liu,[c] Samson Khene,[d] Qing Li,[b] Tawanda Mugadza,[e] Elise Deunf,[f] Tebello Nyokong,[d] and Shaowei W. Chen*[c]

The effects of different redox mediators on the oxygen reduction reaction (ORR) catalyzed by an iron porphyrin complex, iron(III) *meso*-tetra(*N*-methyl-4-pyridyl)porphine chloride [$Fe^{III}$TMPyP], in 0.1 M triflic acid were investigated by cyclic voltammetry (CV) and spectroelectrochemistry in conjunction with density functional theory (DFT) calculations. The formal potentials of the $Fe^{III}$TMPyP catalyst and the redox mediators, as well as the half-wave potentials for the ORR, were determined by CV in the absence and presence of oxygen in acidic solutions. UV/Vis spectroscopic and spectroelectrochemical studies confirmed that only the 2,2′-azino-bis(3-ethylbenzothiazioline-6-sulfonic acid)diammonium salt ($C_{18}H_{24}N_6O_6S_4$) showed effective interactions with $Fe^{III}$TMPyP during the ORR. DFT calculations suggested strong interaction between $Fe^{III}$TMPyP and the $C_{18}H_{24}N_6O_6S_4$ redox mediator. The redox mediator caused lengthening of the dioxygen iron bond, which thus suggested easier dioxygen reduction. Consistent results were observed in electrochemical impedance spectroscopic measurements for which the electron-transfer kinetics were also evaluated.

## 1. Introduction

The recent surge of interest in non-noble-metal porphyrin and phthalocyanine catalysts has been prompted by their potential to replace Pt as cathodic catalysts in polymer electrolyte membrane fuel cells (PEMFCs).[1–3] However, to realize the apparent benefits of the metal–N-coordinated catalysts in high-power fuel cells, advances in catalyst design and synthesis are required to produce catalysts with high turnover rates,[4] and methods of incorporating molecular catalysts into membrane electrode assemblies must be developed. With these advances, the site density can be increased to levels that support high current densities. One approach is to build a 3D, molecular polymer redox layer on the electrode surfaces.[5] The polymer redox layer includes a molecular catalyst, and this structure results in full access to all species (electrons, protons, and substrates) with increased reaction rates. In our previous studies,[1,5,6] we proposed a polymer redox film having a non-noble-metal complex impregnated with Nafion as a new cathode catalyst layer for PEMFCs. In particular, a non-noble-metal catalyst (metal porphyrins) binds with the sulfonic acid sites of Nafion to form a 3D molecular catalyst, and the polymer redox film is attached to the electrode surface.

In the above system, the electrons are transported from the electrode through the catalytic sites, whereas the protons/oxygen atoms migrate along with the hydrophilic domains of Nafion. The water molecules produced by electrochemical reactions move to the polymer surface to form a parasitic liquid water layer. Note that the metal porphyrin complexes are chemically bonded with the sulfonic acid sites of Nafion, and the catalyst is unlikely to migrate. In general, the electron movement is slow among the separate metallic sites, which may be facilitated by the addition of redox mediators with shuttling motions among the active catalytic sites.

In addition to the intrinsic activity of the catalysts for the oxygen reduction reaction (ORR), redox mediators (RMs) also play a crucial role in effective charge transfer.[7] As such, it is important to understand the kinetics of the ORR in the proposed 3D molecular catalyst with suitable RMs. Herein, the effects of RMs on the ORR were tested by using cyclic voltammetry in a homogeneous catalytic system by employing a water-soluble metal macrocycle compound (iron porphyrin) in a triflic acid solution to mimic the 3D catalyst layer. Surprisingly, (dimethylaminomethyl)ferrocene did not show any enhancement for

[a] *Dr. Q. He*
*Department of Molecular & Medical Pharmacology*
*University of California*
*Los Angeles, CA 90095 (USA)*
*E-mail: QHe@mednet.ucla.edu*

[b] *Dr. G. Wu, Dr. Q. Li*
*Materials Physics and Application Division*
*Los Alamos National Laboratory*
*Los Alamos, NM 87545 (USA)*

[c] *K. Liu, Prof. Dr. S. W. Chen*
*Department of Chemistry and Biochemistry*
*University of California*
*1156 High Street, Santa Cruz, CA 95064 (USA)*
*E-mail: shaowei@ucsc.edu*

[d] *Dr. S. Khene, Dr. T. Nyokong*
*Department of Chemistry, Rhodes University*
*P.O. Box 94, Grahamstown, 6140 (South Africa)*

[e] *Dr. T. Mugadza*
*Department of Chemical Technology*
*Midlands State University*
*P. Bag 9055, Gweru (Zimbabwe)*

[f] *Dr. E. Deunf*
*Environmental Energy Technologies Division*
*Lawrence Berkeley National Laboratory*
*1 Cyclotron Road, Berkeley, CA 94720 (USA)*

  

the ORR catalyzed by the iron porphyrin compound, although it did exhibit a more positive formal potential than that exhibited by the catalyst. In situ UV/Vis spectroelectrochemistry was performed to elucidate the possible reasons. Consistent results were obtained in electrochemical impedance spectroscopy (EIS) measurements. In this work, density functional theory (DFT) calculations are used to demonstrate the interaction of $C_{18}H_{24}N_6O_6S_4$ with iron(III) *meso*-tetra(*N*-methyl-4-pyridyl)porphine chlorid ($Fe^{III}$TMPyP) to explain the observed low potential reduction of $O_2$ compared to that of other redox mediators.

## 2. Results and Discussion

### 2.1. Cyclic Voltammetry and Rotating Disk Electrode

The cyclic voltammograms of $Fe^{III}$TMPyP dissolved in 0.1 M triflic acid with different RMs in the absence and presence of $O_2$ are shown in Figure 1 a–c. Well-defined $Fe^{III}/^{II}$TMPyP, RM($n-1$)/RM($n$) redox couples can be observed (see the corresponding insets in the Figure). The formal potentials ($E^{o\prime}$) for $Fe^{III}$TMPyP and the RMs are listed in Table 1. The electrochemical response of the iron porphyrin + RM systems was changed after the triflic acid electrolyte was saturated with oxygen. From Figure 1 a–c it can be seen that in the absence of RMs, the onset potential for the ORR is identical to the potential at which $Fe^{III}$TMPyP is reduced. This result indicates that the ORR process follows a general catalytic regeneration mechanism.[8–10] It is interesting to note that the ORR curves change in quite distinct ways upon the addition of different RMs. For $C_{18}H_{24}N_6O_6S_4$ (Figure 1 a), the half-wave potential ($E_{1/2}$)[11–13] for the ORR is shifted to a significantly more positive position. In contrast, for $[Ru(NH_3)_6]Cl_3$ (Figure 1 b) and $Fe(CH_2NMe_2)$ (Figure 1 c), a negative shift in the $E_{1/2}$ values ($\Delta E_{1/2}$) is observed, as summarized in Table 1. $E_{1/2}$ is an important parameter to evaluate the intrinsic catalytic function for the ORR.[14–16] As such, the marked difference in the shift of $E_{1/2}$ for different RMs unequivocally reveals their varied functions during the ORR catalyzed by $Fe^{III}$TMPyP.

As shown in Figure 2, the ORR activity and four-electron selectivity of the $Fe^{III}$TMPyP catalyst with adding various mediators are determined by using the rotating ring-disk electrode (RRDE) technique. An enhancement in the ORR activity on the $Fe^{III}$TMPyP catalyst was observed if $C_{18}H_{24}N_6O_6S_4$ was added into the electrolyte. Especially, $C_{18}H_{24}N_6O_6S_4$ plays a promotional role in reducing the overpotential of the ORR, as evidenced by positive shifts in the potential in the kinetic range. However, addition of the redox mediators plays an insignificant role in altering the ring current density during the ORR. Thus, appropriate redox mediators are able to accelerate the reaction kinetics, but they cannot further improve the four-electron selectivity during the ORR.

The electrocatalytic activity of the $Fe^{III}$TMPP catalyst was studied as a function of the disk rotation rate ranging from 400 to 1600 rpm. The Koutecky–Levich plots measured with different mediators at 0.078 V are shown in Figure 3. In the Koutecky–Levich equation for a film electrode, the overall measured ORR current $j$ is related to the kinetic current $j_k$ and the boundary-layer diffusion-limiting current $j_d$. The limiting current, $j_d$ can be expressed as [Eq. (1)]:

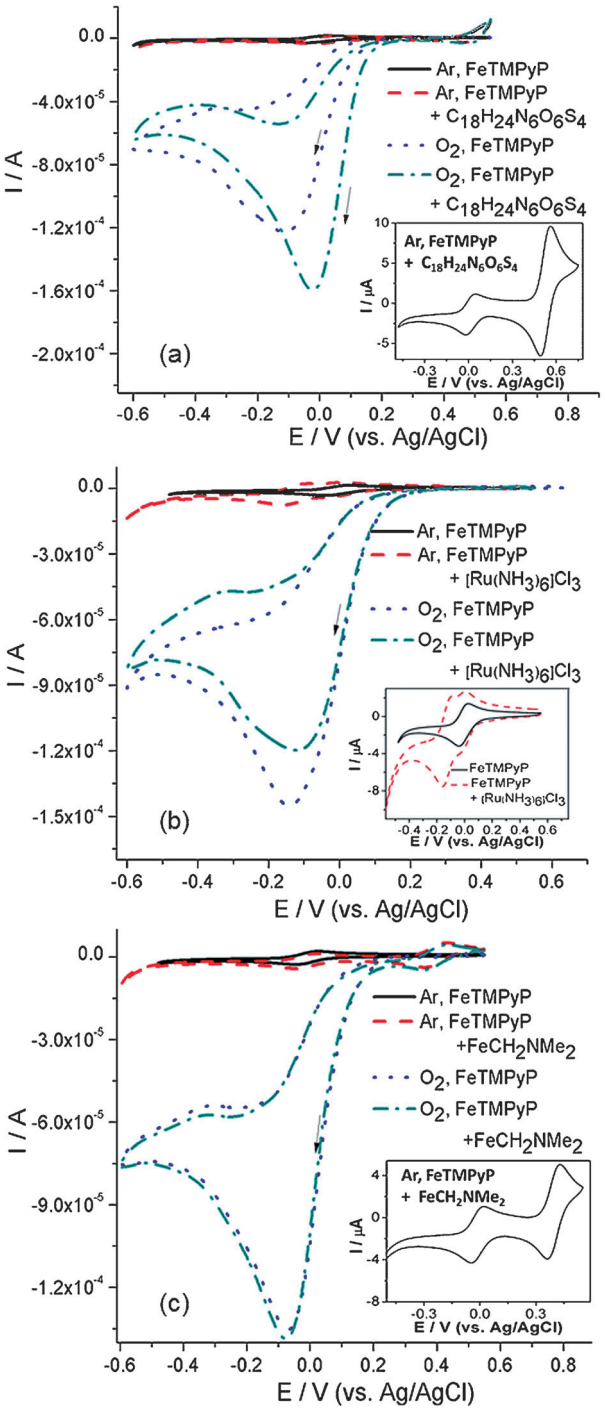


**Figure 1.** Cyclic voltammograms on a glassy carbon electrode in Ar- and $O_2$-purged 0.1 M triflic acid containing 0.2 mM $Fe^{III}$TMPyP in the absence and presence of a) 0.2 mM 2,2′-azino-bis(3-ethylbenzothiazoline-6-sulfonic acid)-diammonium salt, b) 0.2 mM hexaammineruthenium(III) chloride, and c) (dimethylaminomethyl)ferrocene; scan rate = 20 mV $s^{-1}$. Insets) Cyclic voltammograms on the same glassy carbon electrode in Ar-purged 0.1 M triflic acid containing 0.2 mM $Fe^{III}$TMPyP in the presence of 0.2 mM 2,2′-azino-bis(3-ethylbenzothiazoline-6-sulfonic acid)diammonium salt, 0.2 mM hexaammineruthenium(III) chloride, and 0.2 mM (dimethylaminomethyl)ferrocene; potential scan rate = 20 mV $s^{-1}$.

**Table 1.** Formal potential ($E^{o'}$) of different redox mediators and the shift in the half-wave potential ($\Delta E_{1/2}$) of the ORR.

| | $E^{o'}$ [V vs. Ag/AgCl] | $\Delta E_{1/2}$ [mV] |
|---|---|---|
| $Fe^{III}TMPyP$ | −0.014 | 0 |
| $C_{18}H_{24}N_6O_6S_4$ | 0.525 | 59.1 |
| $Ru(NH_4)_6Cl_3$ | −0.125 | −8.3 |
| $FeCH_2NMe_2$ | 0.396 | −9.7 |

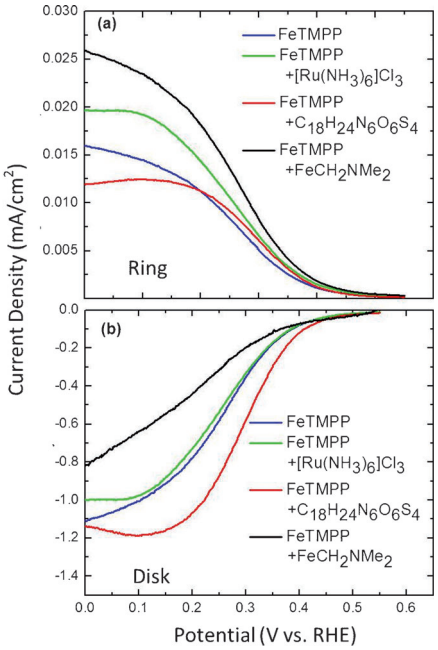


**Figure 2.** RRDE tests for the ORR on the $Fe^{III}TMPP$ catalyst with adding various redox mediators. a) Ring current density representing $H_2O_2$ yields; b) disk current density exhibiting the catalytic activity.

$$j_d = 0.2nFD_O^{2/3}C_O\nu^{-1/6}\omega^{1/2} \quad (1)$$

in which $F$ is the Faraday constant, $D_O$ is the diffusion coefficient of $O_2$ ($1.9\times10^{-5}$ $cm^2s^{-1}$), $\omega$ is the electrode rotation rate in rpm, $\nu$ is the kinematic viscosity of water (0.01 $cm^2s^{-1}$), and $C_O$ is the concentration of $O_2$ in dilute aqueous solution ($1.1\times10^{-6}$ mol $cm^{-3}$). The relationship between the measured current density and the rotation rate is given by [Eq. (2)]:

$$\frac{1}{j} = \frac{1}{j_k} + \frac{1}{j_d} = \frac{1}{j_k} + \frac{1}{B\omega^{1/2}} = A + \frac{1}{B\omega^{1/2}} \quad (2)$$

in which both $A$ and $B$ are constants. On the basis of Equations (1) and (2), the number of electrons transferred in the ORR can be obtained from the slope of the $1/j$ versus $1/\omega^{1/2}$ lines [Eq. (3)]:[17]

$$B = 0.2nFD_O^{2/3}C_O\nu^{-1/6} = 3.5\times10^{-5}n \quad (3)$$

The slopes of the Koutecky–Levich plots in Figure 3 revealed an $n$ value of 3.5 with the $Fe^{III}TMPP$ catalyst. After the addition of $C_{18}H_{24}N_6O_6S_4$, $n$ increased to 3.8. Consequently, the ORR selectivity was significantly improved with the assistance of diammonium relative to other mediators studied in this work, which is in good agreement with the above-discussed ORR activity. In contrast, $n$ decreased to 3.3 upon the addition of $FeCH_2NMe_2$, which indicates the negative impact of $FeCH_2NMe_2$ on the ORR activity on FeTMPP.

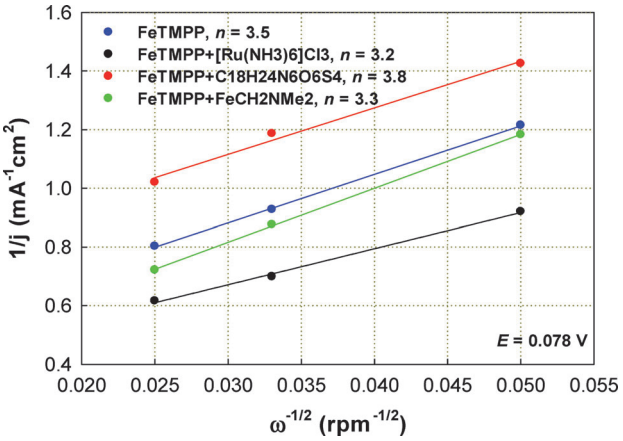


**Figure 3.** Koutecky–Levich plots for the ORR on the $Fe^{III}TMPP$ catalyst with various redox mediators added.

## 2.2. Spectroelectrochemical Studies

It is known that the above RMs have no effect on the ORR potential by themselves. Then one may ask why the ORR proceeds so differently in the electrolytic solution containing $Fe^{III}TMPyP$ together with RMs. To decipher the mechanisms, we used UV/Vis spectroscopy and electrochemistry simultaneously to investigate whether RMs and $Fe^{III}TMPyP$ interact during the ORR process.

The UV/Vis spectrum of $Fe^{III}TMPyP$ in triflic acid (pH 1) exhibits a Soret band at 402 nm, as seen in Figure 4. Upon reducing the solution at −0.2 V (vs. Ag/AgCl), an increase in the intensity and a redshift (415 nm) of the Soret band was evident, which is a common phenomenon that has been observed else-

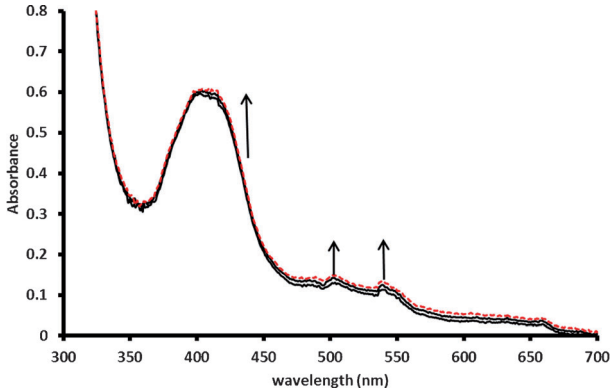


**Figure 4.** UV/Vis spectra for $Fe^{III}TMPyP$ in triflic acid (pH 1) before (——) and after (-----) electrolysis in an OTTLE cell at $E = -0.2$ V.

where,[6,18] and it corresponds to the reduction of $Fe^{III}$TMPyP to $Fe^{II}$TMPyP.

A similar variation of the Soret band was also observed if selected RMs were added into the $Fe^{III}$TMPyP solution. As depicted in Figure 5, upon the addition of an equal volume of 0.5 mM $C_{18}H_{24}N_6O_6S_4$ into a 0.2 mM $Fe^{III}$TMPyP solution, the dark brown iron(III) porphyrin color turned bluish-green (Figure 5, curve ii). Such a change in color is a reflection of the

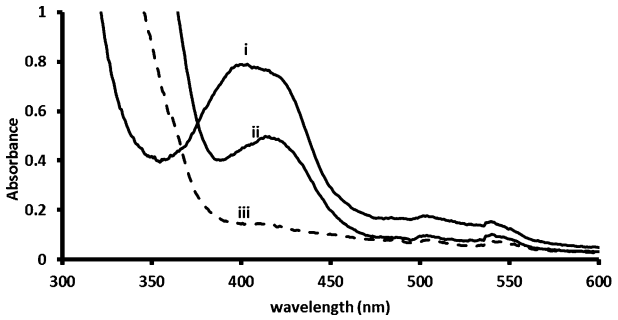


**Figure 5.** UV/Vis spectra of $Fe^{III}$TMPyP (i), the mixture of $Fe^{III}$TMPyP and 2,2′-azino-bis(3-ethylbenzothiazioline-6-sulfonic acid) diammonium salt (ii), and 2,2′-azino-bis(3-ethylbenzothiazioline-6-sulfonic acid) diammonium salt (iii), all in triflic acid solution (pH 1).

reduction of $Fe^{III}$ to $Fe^{II}$, similar to that observed for the nitrosylation of $Fe^{III}$ porphyrins;[18] furthermore, a new Soret band emerged at 415 nm. The shift in the peak position of the Soret band, as compared to that of $Fe^{III}$TMPyP alone (Figure 5, curve i; note that no apparent absorption band is observed with $C_{18}H_{24}N_6O_6S_4$, Figure 5, curve iii) indicated apparent interactions between the $Fe^{III}$ metal center of the porphyrin ($Fe^{III}$TMPyP) and the 2,2′-azino-bis(3-ethylbenzothiazioline-6-sulfonic acid)diammonium salt. A concurrent decrease in the absorbance of the mixture was also observed, possibly due to strong interactions between $Fe^{III}$ and the RM and hence a significant change in the molecular structures.

Upon the application of a reducing potential to the $Fe^{III}$TMPyP and $Ru(NH_3)_6Cl_3$ mixture ($E=-0.2$ V), there was no fundamental change in the spectra, as shown in Figure 6, except for a slight broadening of the Soret band; this suggests that there was virtually no direct interaction between $Fe^{III}$TMPyP and $Ru(NH_3)_6Cl_3$. This result is in agreement with the measurements of the redox potentials that show that $[Ru(NH_3)_6]Cl_3$ has a more negative redox potential than $Fe^{III}$TMPyP and, therefore, cannot reduce it. As a result, it is

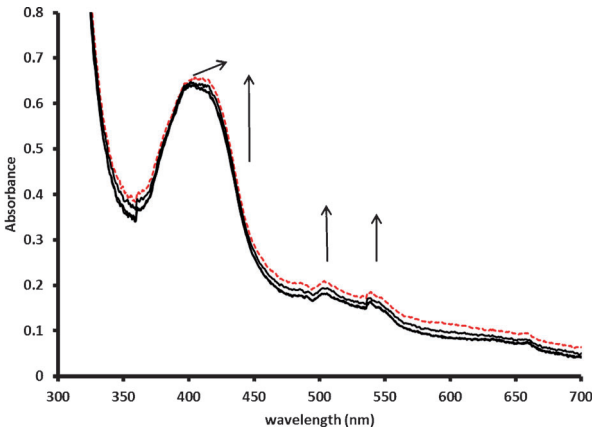


**Figure 6.** UV/Vis absorption spectra for the $Fe^{III}$TMPyP and hexaammineruthenium(III) chloride mixture before (——) and after (-----) electrolysis at $E=-0.2$ V in triflic acid (pH 1).

not surprising to see that there is no enhancement in the ORR.

Similar to acid salts, one may expect that $Fe^{III}$ can be reduced by $FeCH_2NMe_2$ due to the high redox potential of $FeCH_2NMe_2$. However, from Figure 1c it is surprising to see that the ORR was actually somewhat inhibited in the presence of $FeCH_2NMe_2$. To address this phenomenon, in situ UV/Vis spectra were recorded at different potentials in a triflic acid solution containing $Fe^{III}$TMPyP and $FeCH_2NMe_2$. Interestingly, in Figure 7 no new band evolved, but the band density at 405 nm decreased with an increasingly negative electrode potential. From the inset in Figure 7, the main band at 405 nm in the UV/Vis curves of $Fe^{III}$TMPyP and the $Fe^{III}$TMPyP + $FeCH_2NMe_2$ mixture overlap with each other, which indicates that there was no interaction between $Fe^{III}$TMPyP and

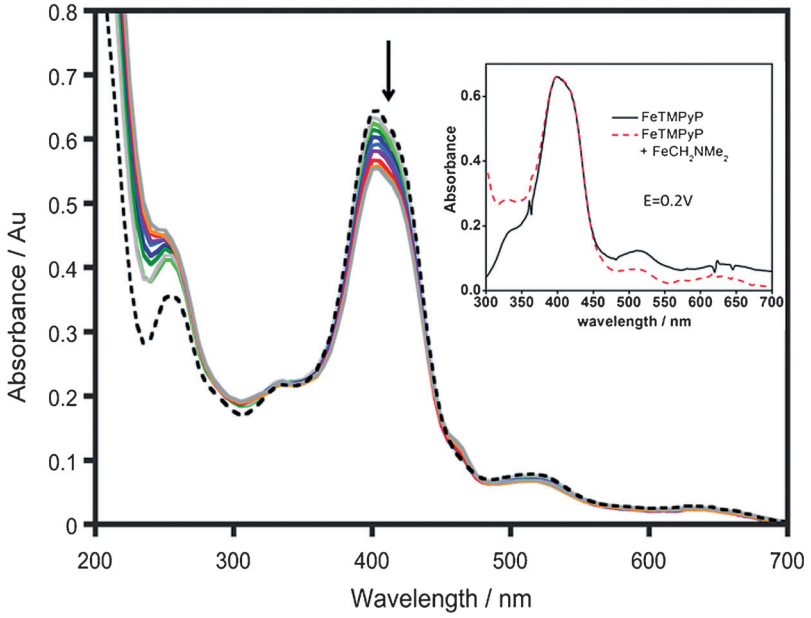


**Figure 7.** UV/Vis spectrograms recorded before and after 10 min controlled-potential coulometry at increasing applied potentials: 0.15, 0.10, 0.05, 0.00, −0.05, −0.15, −0.20, and −0.25 V versus Ag/AgCl in a triflic acid solution of $Fe^{III}$TMPyP and $FeCH_2NMe_2$. Inset) Spectra for $Fe^{III}$TMPyP (——) and $Fe^{III}$TMPyP + $FeCH_2NMe_2$ mixture (-----) at $E=+0.2$ V.

$FeCH_2NMe_2$ in the acidic solution over a broad potential window.

### 2.3. EIS Study

The electron-transfer kinetics of the ORR were then examined by EIS measurements. Figure 8 shows the Nyquist complex-plane impedance spectra of the ORR at varied potentials with the iron porphyrin catalyst alone and with the addition of the three selected redox mediators in an $O_2$-saturated 0.1 M triflic acid solution. In all four systems under study, generally the EIS spectra exhibit a single semicircle, which suggests that under the current experimental conditions the interfacial kinetics of the ORR process is the predominant step for the electrode reactions.[13]

For each system under study, it can be clearly seen that the diameter of the arc decreased with a cathodic shift in the applied potential. This observation is consistent with the voltammetric results in Figure 1. As the diameter of the impedance arc represents the charge-transfer resistance ($R_{CT}$) of the ORR at the electrode surface, a decrease in the diameter of the arc suggests enhanced electron-transfer kinetics, as shown in Figure 8. In addition, the diameters of the impedance arcs in the presence of iron porphyrin and $C_{18}H_{24}N_6O_6S_4$ are clearly smaller than those in other systems over the entire potential range from $+0.3$ to $-0.2$ V, which suggests lower charge-transfer resistance and higher oxygen-reduction activity.

The equivalence circuit shown in the inset of Figure 9 was then used to fit the impedance data, for which $R_S$ represents the solution resistance and $C_{DL}$ and $R_{CT}$ are the double-layer capacitance and charge-transfer resistance, respectively. The overall variation in the charge-transfer resistance ($R_{CT}$) with different applied potentials is depicted in Figure 9. First, for all systems under study, $R_{CT}$ decreased as the potential was moved negatively; this is indicative of enhanced oxygen-reduction kinetics. Second, it can be seen that over the entire potential range, $R_{CT}$ is noticeably smaller with iron porphyrin and $C_{18}H_{24}N_6O_6S_4$ than with other systems. For instance, at about $+0.04$ V, the value of $R_{CT}$ for the iron porphyrin catalyst is 8.52 kΩ, and the addition of $C_{18}H_{24}N_6O_6S_4$ lowered the value to 3.27 kΩ, whereas in the presence of $[Ru(NH_3)_6]Cl_3$ and Fe-($CH_2NMe_2$), the $R_{CT}$ values are also lower but to a much less extent at 7.49 and 6.92 kΩ, respectively. These behaviors are consistent with the voltammetric results. That is, within the present experimental context, $C_{18}H_{24}N_6O_6S_4$ exhibited the most significant enhancement for the ORR electrocatalytic activity of iron porphyrin in acidic media.

### 2.4. DFT Studies

Figure 1 a shows that the reduction of dioxygen is significantly more influenced by the $C_{18}H_{24}N_6O_6S_4$ redox mediator than by other redox mediators (Figure 1 b, c). The reduction potential of dioxygen in the presence of the $[Ru(NH_3)_6]Cl_3$ and $Fe(CH_2NMe_2)$ redox mediators shows similar behavior, which thus suggests minimal interaction between the catalyst and the redox mediators. DFT calculations were performed to investigate the interaction of dioxygen and the $C_{18}H_{24}N_6O_6S_4$ redox mediator with $Fe^{III}$TMPyP $[O_2Fe^{III}(C_{18}H_{24}N_6O_6S_4)]$. Figure 10 shows the optimized structures of the $O_2Fe^{III}(C_{18}H_{24}N_6O_6S_4)$ and $O_2Fe^{III}(OH)$ complexes. The OH group was used in place of Cl to simplify the DFT calculations.

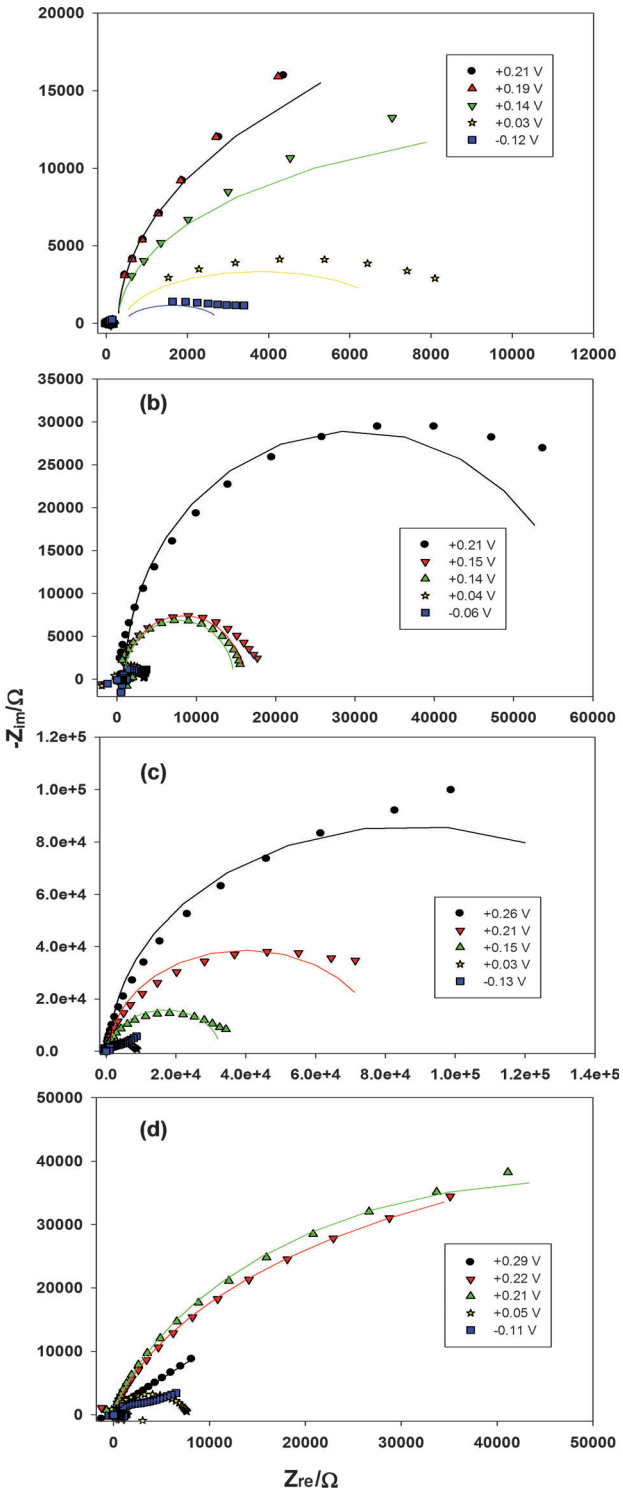


**Figure 8.** Complex plane (Nyquist) impedance plots of oxygen reduction catalyzed by iron porphyrin a) in the absence of RMs and in the presence of b) $C_{18}H_{24}N_6O_6S_4$, c) $[Ru(NH_3)_6]Cl_3$, and d) $FeCH_2NMe_2$ at different electrode potentials (shown in the figure legends). Symbols are experimental data and lines are simulations based on the equivalent circuits shown in Figure 9

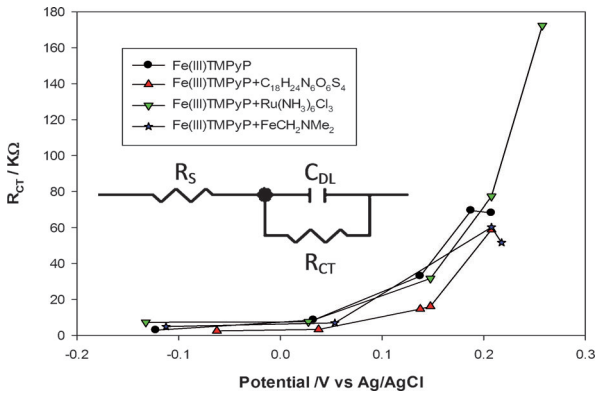


**Figure 9.** Variations in the charge-transfer resistance ($R_{CT}$) with electrode potentials in oxygen reduction catalyzed by $Fe^{III}$TMPyP in the absence and presence of various redox mediators. Data were obtained by curve fitting of the impedance spectra (Figure 8) according to the equivalent circuit shown in the inset.

The modeled porphyrin dioxygen adduct (Figure 10a, b) shows what is referred to as a side on adsorption of dioxygen with respect to the central mental. (Figure 9a shows that the redox mediator can coordinate to the central metal ion thus to form an octahedral complex). Because there are no other redox mediators for oxygen to coordinate with, the Fe central metal cannot displace the Cl atom, and this results in similar reduction potentials observed for dioxygen. The DFT calculations and the electrochemical data allow the following reaction schemes to be proposed [Eqs. (4)–(9)]:

$$Cl - Fe^{III}TMPy + \text{redox mediator} \rightleftharpoons Cl - Fe^{II}TMPyP - \text{redox mediator} \quad (4)$$

$$Cl - Fe^{II}TMPyP - \text{redox mediator} + O_2 \rightleftharpoons O_2 - Fe^{II}TMPYP - \text{redox mediator} + Cl^- \quad (5)$$

$$O_2 - Fe^{II}TMPyP - \text{redox mediator} + e^- \rightarrow O_2^- - Fe^{III}TMPyP - \text{redox mediator} \quad (6)$$

$$O_2^- - Fe^{III}TMPyP - \text{redox mediator} + e^- \rightarrow O_2^- - Fe^{II}TMPyP - \text{redox mediator} \quad (7)$$

$$O_2^- - Fe^{II}TMPyP - \text{redox mediator} + H_3^+O \rightarrow Fe^{III}TMPyP - \text{redox mediator} + H_2O_2 \quad (8)$$

$$2\,Fe^{III}TMPyP - \text{redox mediator} + H_2O_2 + 2\,H_3^+O + 2\,e^- \rightarrow 2\,Fe^{IV} + 4\,H_2O \quad (9)$$

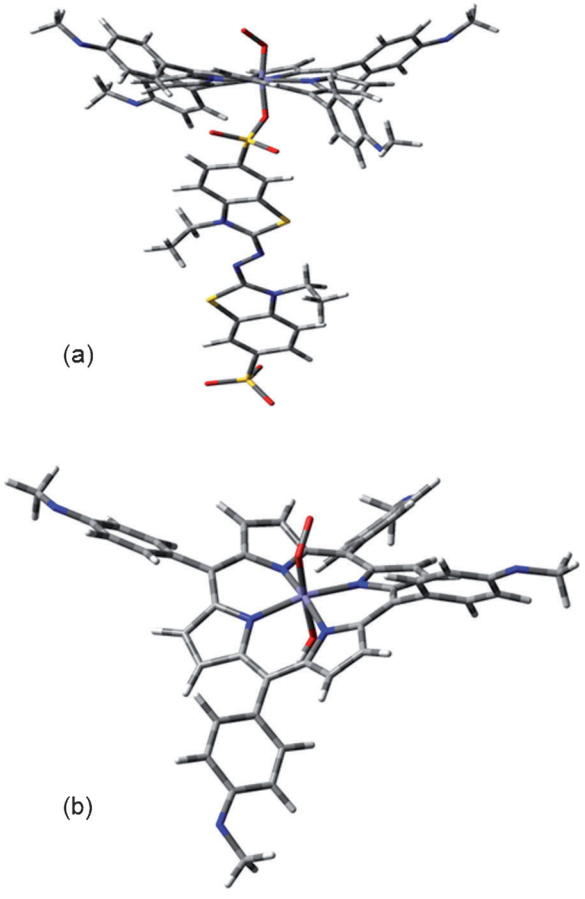


**Figure 10.** Optimized structure of a) $O_2Fe^{III}(C_{18}H_{24}N_6O_6S_4)$ and b) $O_2Fe^{III}(OH)$ calculated at B3LYP/SDD.

The $C_{18}H_{24}N_6O_6S_4$ redox mediator reacts reversibly with $ClFe^{III}$TMPy to form a reduced species indicated as $ClFe^{II}$TMPy–redox mediator adduct. This step is confirmed by the observed redshift in the Soret band (Figure 5) and by color changes in the solution (from dark brown to bluish-green) upon the addition of the redox mediator to the $Fe^{III}$TMPyP solution. The next step involves a reaction of dioxygen with the $ClFe^{II}$TMPy–redox mediator adduct to form the $O_2Fe^{III}$TMPy–redox mediator adduct. It is known that the ligand coordinated to the leaving group lowers the activation energy for the substitution reaction by destabilizing the ground state of the complex or by stabilizing the activated complex. Destabilization of the ground state by $C_{18}H_{24}N_6O_6S_4$ due to strong σ-electron donation along the $C_{18}H_{24}N_6O_6S_4$—Fe–Cl axis promotes the weakening of the Fe–Cl bond; this makes dissociation easier and leads to substitution of dioxygen. The $C_{18}H_{24}N_6O_6S_4$ redox mediator is also coordinated to the dioxygen group in the $O_2Fe^{II}$TMPy–redox mediator adduct. The next step is the formation of the superoxide ion with iron in a ferric state ($O_2^-Fe^{III}$TMPy–redox mediator adduct). The next step involves the reduction of the $O_2^-Fe^{III}$TMPy–redox mediator adduct at negative potentials, which results in the reduction of the dioxygen adduct to $^-O_2Fe^{II}$TMPy–redox mediator. In acidic solution, the adduct is converted into $Fe^{III}$TMPy–redox mediator and hydrogen peroxide. The final step involves the reaction of $Fe^{III}$TMPy–redox mediator with hydrogen peroxide in acidic media to form $H_2O$ as the final product.

The ease of reduction can be associated with the bond length between Fe and $O_2$. The calculated bond length between the Fe and $O_2$ adduct for $C_{18}H_{24}N_6O_6S_4$ (Figure 10a) and OH (Figure 10b) is 1.77486 and 1.71575 Å, respectively. The bond length for dioxygen in the $O_2Fe^{III}$TMPy–redox mediator adduct is longer than that in the $O_2$FeTMPy–OH adduct. This

observation suggests that the σ electron density of $C_{18}H_{24}N_6O_6S_4$ promotes the weakening of the Fe–$O_2$ bond, which thus makes dioxygen reduction easier. The *trans* ligand seems to facilitate the oxygen-reduction process through the *trans* effect. This observation from DFT calculation correlates well with the experimental observation of lower reduction potentials for dioxygen in the presence of the $C_{18}H_{24}N_6O_6S_4$ redox mediator.

## 3. Conclusions

Three selected redox mediators including 2,2′-azino-bis(3-ethylbenzothiazoline-6-sulfonic acid)diammonium salt ($C_{18}H_{24}N_6O_6S_4$), hexaammineruthenium(III) chloride ([Ru($NH_3$)$_6$]$Cl_3$), and (dimethylaminomethyl)ferrocene ($FeCH_2NMe_2$) were investigated in the catalytic reduction of oxygen by iron porphyrin [$Fe^{III}$TMPyP] in acidic media. Except for [Ru($NH_3$)$_6$]$Cl_3$, all redox mediators exhibited formal potentials more positive than that of $Fe^{III}$TMPyP. Therefore, it was expected (and observed) that there was no enhancement in the ORR catalyzed by $Fe^{III}$TMPyP with [Ru($NH_3$)$_6$]$Cl_3$. Additionally, $FeCH_2NMe_2$ (with a more positive value of the formal potential) inhibited the ORR in 0.1 M triflic acid + 0.2 mM $Fe^{III}$TMPyP. In marked contrast, a more positive half-wave potential ($E_{1/2}$) for the ORR was observed with $C_{18}H_{24}N_6O_6S_4$. Spectroelectrochemical data revealed that $Fe^{III}$TMPyP was reduced to $Fe^{II}$TMPyP in the presence of $C_{18}H_{24}N_6O_6S_4$, which led to enhanced activity of the ORR. Consistent results were obtained in EIS measurements for which the charge-transfer resistance in the oxygen reduction was found to decrease with the addition of redox mediators, and the best performance among the series was observed with $C_{18}H_{24}N_6O_6S_4$. That is, within the experimental context, $C_{18}H_{24}N_6O_6S_4$ exhibited the most significant enhancement in the ORR activity. DFT calculations were employed to probe the interaction between $Fe^{III}$TMPyP and the $C_{18}H_{24}N_6O_6S_4$ redox mediator. These calculations showed that there was a substantial interaction between $Fe^{III}$TMPyP and the $C_{18}H_{24}N_6O_6S_4$ redox mediator. The redox mediator caused lengthening of the dioxygen iron bond, which thus made dioxygen reduction easier.

## Experimental Section

### General Methods

The iron(III) *meso*-tetra(*N*-methyl-4-pyridyl)porphine chloride ($Fe^{III}$TMPyP) catalyst was obtained from Frontier Scientific, Inc., and was used as received. All other chemical materials including the RMs [2,2′-azinobis(3-ethylbenzothiazoline-6-sulfonic acid)diammonium salt ($C_{18}H_{24}N_6O_6S_4$), hexaammineruthenium(III) chloride ([Ru($NH_3$)$_6$]$Cl_3$), and (dimethylaminomethyl)ferrocene ($FeCH_2NMe_2$)] were analytical grade and were obtained from Sigma–Aldrich. The pH of the 0.1 M triflic acid solution was determined to be 1.0 by using a Beckman Coulter model 510 pH Meter.

### Computational Methods

The Gaussian 03 program[19] running on an Intel/Linux cluster was used to perform DFT calculations. All DFT calculations were performed at the B3LYP level with a basis set SDD for optimization. All visualization used the Gausview 4.1 program.[19]

### Characterization

Cyclic voltammetry measurements were conducted in a standard three-compartment electrochemical cell maintained at room temperature (20–25 °C) by using a rotating disk electrode (RDE) setup from the Pine Instrument Company connected to an Autolab bipotentiostat (PGSTAT302N). A glassy carbon electrode (diameter = 5.61 mm) from the Pine Instrument Company was used as the working electrode. A Pt wire was taken as the counter electrode. A "no leak" Ag/AgCl reference electrode was obtained from Cypress Systems. Before measurement, the RDE was first polished successively with 1.0, 0.3, and 0.05 μm alumina slurries (Buehler, Lake Bluff, IL) and then cleaned with distilled water under sonication. The disk electrode potential was scanned in a defined potential windows at 20 mV $s^{-1}$. EIS measurements were conducted at varied potentials by using an EG&G PARC Potentiostat/Galvanostat (Model 283) in conjunction with a frequency response detector (Model 1025). The impedance spectra were recorded between 10 kHz and 0.1 Hz with an alternating current (AC) signal amplitude of 10 mV.

In the RRDE testing, the ring potential was set to 1.2 V. Before the experiments, the Pt ring was activated by potential cycling in 0.5 M $H_2SO_4$ from 0.0 to 1.4 V at a scan rate of 50 mV $s^{-1}$ for 10 min. The four-electron selectivity of the catalysts was evaluated on the basis of the yield of $H_2O_2$, which was calculated from the following equation [Eq. (10)]:

$$H_2O_2\,[\%] = 200 \times \frac{I_R/N}{(I_R/N) + I_D} \qquad (10)$$

in which $I_D$ and $I_R$ are the disk and ring currents, respectively, and $N$ is the ring collection efficiency, which was calibrated to be 36%.

In situ UV/Vis spectra were collected with a Shimadzu UV-2550 spectrophotometer. Spectroelectrochemical data were obtained by connecting a homemade optically transparent thin-layer electrochemical (OTTLE) cell to a Bioanalytical Systems (BAS) CV 27 voltammograph. All spectroelectrochemical experiments were performed in 0.1 M triflic acid (pH 1). Pt mesh working and auxiliary electrodes and an Ag/AgCl reference electrode were employed for the OTTLE cell.

## Acknowledgements

*This work was supported by the National Science Foundation (CHE-1012258 and CHE-1265635) and the Department of Science and Technology (DST)/National Research Foundation (NRF) South African Research Chairs Initiative (SARChI). We also thank Dr. Frank McLarnon for helpful comments and suggestions during preparation of this manuscript.*

**Keywords:** density functional calculations · homogeneous catalysis · iron · porphyrins · redox mediator

[1] Q. He, T. Mugadza, G. Hwang, T. Nyokong, *Int. J. Electrochem. Sci.* **2012**, *7*, 7045 – 7064.

[2] Q. He, X. Yang, R. He, A. Bueno-Lopez, H. Miller, X. Ren, W. Yang, B. E. Koel, *J. Power Sources* **2012**, *213*, 169 – 179.
[3] S. L. Pimlott, A. Sutherland, *Chem. Soc. Rev.* **2011**, *40*, 149 – 162.
[4] H. A. Gasteiger, S. S. Kocha, B. Sompalli, F. T. Wagner, *Appl. Catal. B* **2005**, *56*, 9 – 35.
[5] X. Zhu, J. B. Kerr, Q. He, G. Hwang, Z. Martin, K. Clark, A. Weber, N. Zhao, *ECS Trans.* **2012**, *45*, 143 – 152.
[6] Q. He, T. Mugadza, X. Kang, X. Zhu, S. Chen, J. Kerr, T. Nyokong, *J. Power Sources* **2012**, *216*, 67 – 75.
[7] E. Kibena, U. Mäeorg, L. Matisen, K. Tammeveski, *J. Electroanal. Chem.* **2011**, *661*, 343 – 350.
[8] C. P. Andrieux, J. M. Dumas-Bouchiat, J. M. Saveant, *J. Electroanal. Chem.* **1978**, *87*, 55 – 65.
[9] C. P. Andrieux, J. M. Dumas-Bouchiat, J. M. Saveant, *J. Electroanal. Chem.* **1978**, *87*, 39 – 53.
[10] C. P. Andrieux, J. M. Dumas-Bouchiat, J. M. Saveant, *J. Electroanal. Chem.* **1978**, *88*, 43 – 48.
[11] N. M. Markovic, R. R. Adzic, B. D. Cahan, E. B. Yeager, *J. Electroanal. Chem.* **1994**, *377*, 249 – 259.
[12] Q. He, S. Mukerjee, S. Parres-Esclapez, A. Bueno-López, *J. Appl. Electrochem.* **2011**, *41*, 891 – 899.
[13] Q. He, X. Yang, W. Chen, S. Mukerjee, B. Koel, S. Chen, *Phys. Chem. Chem. Phys.* **2010**, *12*, 12544 – 1255.
[14] Y.-Y. Feng, J.-H. Ma, G.-R. Zhang, G. Liu, B.-Q. Xu, *Electrochem. Commun.* **2010**, *12*, 1191 – 1194.
[15] Q. He, S. Mukerjee, *Electrochim. Acta* **2010**, *55*, 1709 – 1719.
[16] Z. Gao, Y. H. Lim, M. Tredwell, L. Li, S. Verhoog, M. Hopkinson, W. Kaluza, T. L. Collier, J. Passchier, M. Huiban, V. Gouverneur, *Angew. Chem. Int. Ed.* **2012**, *51*, 6733 – 6737; *Angew. Chem.* **2012**, *124*, 6837 – 6841.
[17] G. Wu, G. Cui, D. Li, P.-K. Shen, N. Li, *J. Mater. Chem.* **2009**, *19*, 6581 – 6589.
[18] N. S. Trofimova, A. Y. Safronov, O. Ikeda, *Inorg. Chem.* **2003**, *42*, 1945 – 1951.
[19] Gaussian 03, Revision E.01, M. J. Frisch, G. W. Trucks, H. B. Schlegel, G. E. Scuseria, M. A. Robb, J. R. Cheeseman, J. A. Montgomery, Jr., T. Vreven, K. N. Kudin, J. C. Burant, J. M. Millam, S. S. Iyengar, J. Tomasi, V. Barone, B. Mennucci, M. Cossi, G. Scalmani, N. Rega, G. A. Petersson, H. Nakatsuji, M. Hada, M. Ehara, K. Toyota, R. Fukuda, J. Hasegawa, M. Ishida, T. Nakajima, Y. Honda, O. Kitao, H. Nakai, M. Klene, X. Li, J. E. Knox, H. P. Hratchian, J. B. Cross, V. Bakken, C. Adamo, J. Jaramillo, R. Gomperts, R. E. Stratmann, O. Yazyev, A. J. Austin, R. Cammi, C. Pomelli, J. W. Ochterski, P. Y. Ayala, K. Morokuma, G. A. Voth, P. Salvador, J. J. Dannenberg, V. G. Zakrzewski, S. Dapprich, A. D. Daniels, M. C. Strain, O. Farkas, D. K. Malick, A. D. Rabuck, K. Raghavachari, J. B. Foresman, J. V. Ortiz, Q. Cui, A. G. Baboul, S. Clifford, J. Cioslowski, B. B. Stefanov, G. Liu, A. Liashenko, P. Piskorz, I. Komaromi, R. L. Martin, D. J. Fox, T. Keith, M. A. Al-Laham, C. Y. Peng, A. Nanayakkara, M. Challacombe, P. M. W. Gill, B. Johnson, W. Chen, M. W. Wong, C. Gonzalez, J. A. Pople, Gaussian, Inc., Wallingford CT, 2004.

Received: March 14, 2014
Published online on July 13, 2014